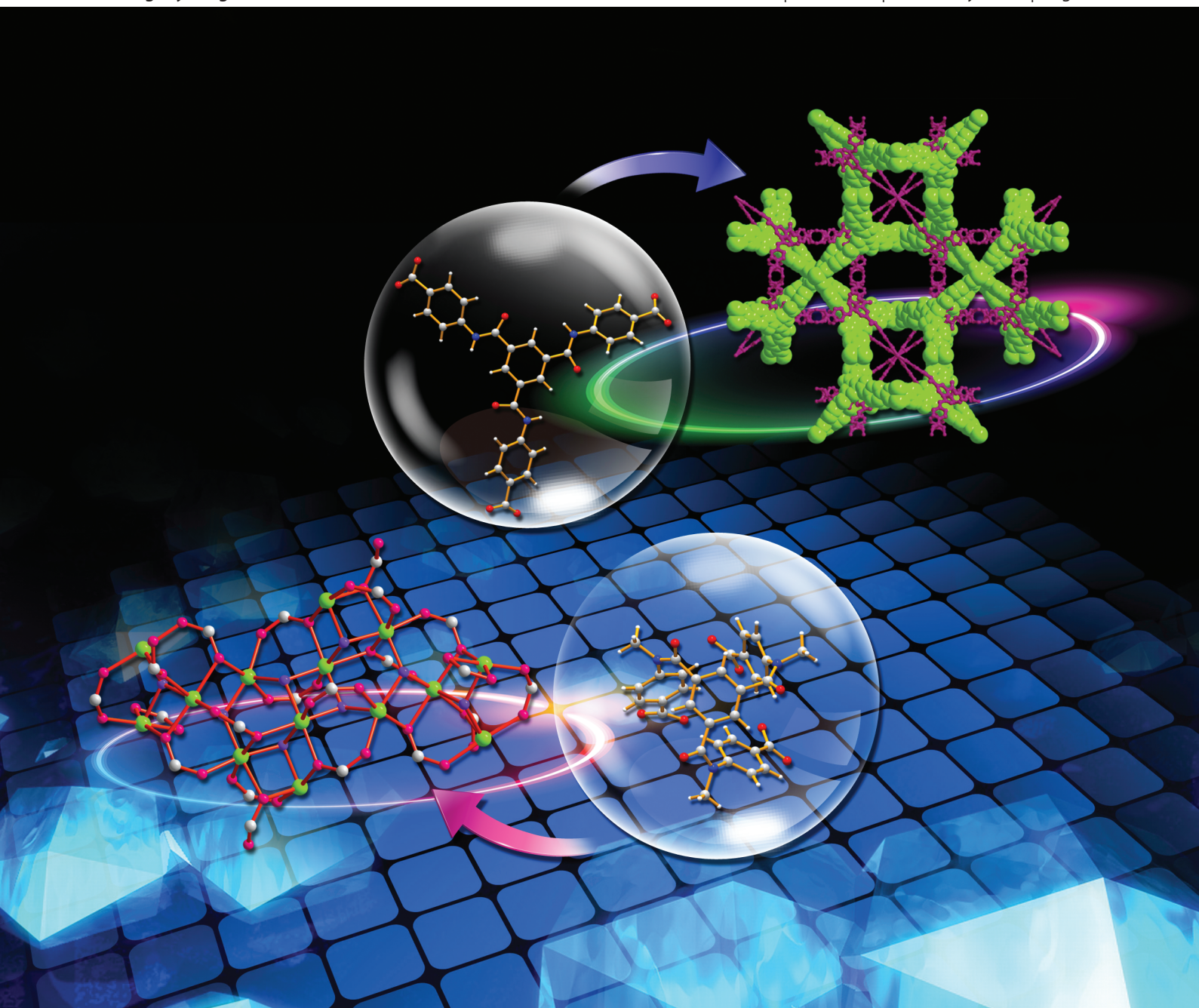


# CrystEngComm

www.rsc.org/crystengcomm

Volume 15 | Number 2 | 14 January 2013 | Pages 215–422



RSC Publishing

**PAPER**

Myoung Soo Lah *et al.*

Conformational control of ligands to create a finite metal–organic cluster and an extended metal–organic framework

# Conformational control of ligands to create a finite metal–organic cluster and an extended metal–organic framework†

Cite this: *CrystEngComm*, 2013, 15, 259

Lalit Rajput, Dongwook Kim and Myoung Soo Lah\*

While a twofold interpenetrated 3-D metal–organic framework,  $[\text{Cu}_3(\text{L}^1)_2(\text{H}_2\text{O})_3] \cdot 14\text{DMF} \cdot 16\text{H}_2\text{O}$  (**1**) (where,  $\text{L}^1$  is 4,4',4''-[1,3,5-benzenetriyltris(carbonylimino)]trisbenzoate and DMF is *N,N'*-dimethylformamide), with a (3,4)-connected **pto** net topology was prepared using a tricarboxylic acid linked *via* secondary benzamide as an extended 3-connected node and a Cu paddle-wheel secondary building unit as a planar 4-connected node, another tricarboxylic acid with methylated tertiary benzamide linkage in a folded geometry completely converted its role from diverging to chelating ligand and resulted in a finite  $\text{Ni}_{14}$  metal–organic cluster,  $[\text{Ni}_{14}(\mu^3\text{-OH})_8(\text{L}^2)_6(\text{formate})_2(\text{DMF})_{10}(\text{H}_2\text{O})_2] \cdot 28\text{DMF} \cdot 14\text{H}_2\text{O}$  (**2**) (where  $\text{L}^2$  is *N,N',N''*-methyl-4,4',4''-[1,3,5-benzenetriyltris(carbonylimino)]trisbenzoate).

Received 26th June 2012,  
Accepted 1st October 2012

DOI: 10.1039/c2ce26015h

[www.rsc.org/crystengcomm](http://www.rsc.org/crystengcomm)

## Introduction

The design and synthesis of metal–organic materials such as finite metal–organic clusters (MOCs) and extended metal–organic frameworks (MOFs) has become a subject of extensive investigation because of their intriguing architectures<sup>1,2</sup> and potential applications.<sup>3,4</sup> The connectivity and symmetry of the constituting metal ion (or metal cluster) and organic ligand often govern the structural characteristics of metal–organic materials.<sup>2</sup> Even a small change in the characteristics of the ligand, such as its conformation, can produce significant differences in the final structure.

The control of the net topology of MOFs can be relatively easily achieved when a rigid ligand with restrained conformation is used as a building block. For example, it is well known that the combination of a tricarboxylic acid as a 3-connected node with a metal ion that can form a planar 4-connected  $\text{M}_2(\text{COO})_4$  secondary building unit (SBU) leads to a (3,4)-connected 3-D network of either a **tbo** net topology<sup>5</sup> or a **pto** net topology,<sup>6</sup> depending on the extent of twisting of the carboxylates from the ligand plane. While a ligand with all the carboxylates in the ligand plane results in a network with a **tbo** net topology, a ligand with carboxylates twisted from the ligand plane forms a network with a **pto** net topology.<sup>7</sup>

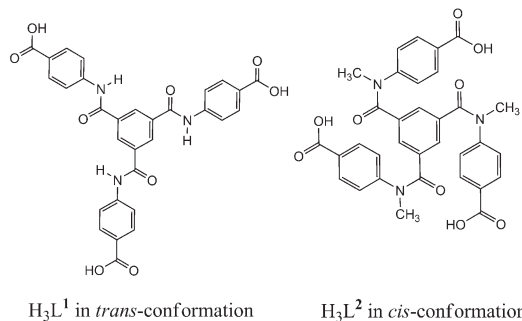
Flexible ligands with more or fewer conformational degrees of freedom could diversify the dimensionality of metal–organic materials and their net topology. Recently, Argent *et al.* reported the preparation of metal–organic materials using a tricarboxylate ligand with some conformational flexibility.<sup>8</sup> Depending on the reaction conditions, a finite metal–organic nanosphere or an extended 1-D or 2-D coordination polymer having different ligand conformations were obtained. However, it is not well understood which factor determines the ligand conformation. The prediction of the final structure from the building components and the reaction conditions is still a difficult task.

It is well known that secondary benzamide has a strong tendency to adopt the *trans*-amide conformation,<sup>9</sup> and in this conformation the amide has an extended geometry with a certain degree of conformational flexibility. On the other hand, alkylated tertiary benzamide adopts the *cis*-amide conformation, which leads to a folded geometry.<sup>9</sup> In the present work, we investigate how the conformational preference and the flexibility of the amide-linked tricarboxylate ligand could be utilized in the synthesis of metal–organic materials. We chose 4,4',4''-[1,3,5-benzenetriyltris(carbonylimino)]trisbenzoic acid ( $\text{H}_3\text{L}^1$ ) as a ligand having a secondary amide linkage<sup>10</sup> and synthesized its methylated analogue, *N,N',N''*-methyl-4,4',4''-[1,3,5-benzenetriyltris(carbonylimino)]trisbenzoic acid ( $\text{H}_3\text{L}^2$ ), as another ligand containing tertiary amide linkages. Ligand  $\text{H}_3\text{L}^1$  in a *trans*-amide conformation and with a consequently extended geometry will serve as a 3-connected node, while  $\text{H}_3\text{L}^2$  in a *cis*-amide conformation and with a folded geometry could serve as a folded tripodal ligand (Scheme 1). It was reported that  $\text{H}_3\text{L}^1$  in an extended conformation led to a 3-D network of a (3,6)-

Interdisciplinary School of Green Energy, Ulsan National Institute of Science & Technology, Ulsan, 689-798, Korea. E-mail: mslah@unist.ac.kr;

Fax: +82 52 217 2019; Tel: +82 52 217 2931

† Electronic supplementary information (ESI) available: Tables of crystal data and structure refinement, crystallographic information files in CIF format, and PXRD data. CCDC 888899 and 888900. For ESI and crystallographic data in CIF or other electronic format see DOI: 10.1039/c2ce26015h



**Scheme 1** Secondary benzamide in *trans*-conformation and tertiary benzamide in *cis*-conformation.

connected **rtl** net topology when it was combined with a 6-connected tetranuclear  $\text{Zn}_4\text{O}(\text{COO})_6$  SBU.<sup>10</sup> However,  $\text{H}_3\text{L}^2$  in a folded tripodal geometry could direct to a finite MOC or metal-organic materials of low dimensionality. Here, we describe the syntheses and structural characterizations of two metal-organic materials based on Cu(II) and Ni(II) metal ions by using the two amide-linked tricarboxylic acids,  $\text{H}_3\text{L}^1$  with an extended geometry and  $\text{H}_3\text{L}^2$  with a folded geometry.

## Experimental section

### General procedures

All reagents were purchased from commercial sources and were used without further purification. Elemental analysis (EA) (C, H, and N) was performed using a Thermo Scientific Flash 2000 elemental analyzer. Infrared spectra were recorded over the range 4000–600  $\text{cm}^{-1}$  using a Varian 670 FT-IR spectrophotometer. Nuclear magnetic resonance (NMR) spectra were obtained on a Varian-600 NMR spectrometer. Powder X-ray diffraction (PXRD) data were recorded using a Rigaku D/M 2200T automated diffractometer at room temperature using a step size of 0.02°. Simulated PXRD patterns were calculated using the Material Studio software package<sup>11</sup> employing single crystal data.  $\text{H}_3\text{L}^1$  was prepared according to the literature procedure.<sup>10</sup>

### Synthesis of *N,N',N''*-methyl-4,4',4''-[1,3,5-benzenetriyltris(carboxylimino)]trisbenzoic acid ( $\text{H}_3\text{L}^2$ )

**4-METHYLAMINOBENZOIC ACID METHYL ESTER.** 2.502 g (16.55 mmol) of 4-methylaminobenzoic acid was dissolved in 120 mL of dry methanol and cooled to 0 °C in an ice bath. To the above solution, 1.85 mL (25.5 mmol) of  $\text{SOCl}_2$  was added dropwise. After complete addition of  $\text{SOCl}_2$ , the reaction mixture was refluxed for 3 h. The reaction mixture was cooled to ambient temperature, quenched with saturated  $\text{NaHCO}_3$  at 0 °C and extracted with ethyl acetate. The organic layer was washed using brine, dried with anhydrous sodium sulfate and evaporated to give a white solid product. Yield = 2.424 g, 88.71%. <sup>1</sup>H NMR ( $\text{CDCl}_3$ ,  $\delta$  ppm): 2.89 (s, 3H), 3.85 (s, 3H), 4.35 (s, 1H), 6.56 (d, 2H), 7.88 (d, 2H).

***N,N',N''*-METHYL-4,4',4''-[1,3,5-BENZENETRIYLTRIS(CARBONYLIMINO)]TRISBENZOIC ACID METHYL ESTER.** 0.929 g (3.50 mmol) of 1,3,5-benzenetricarboxylic acid chloride was added to a solution of 1.714 g (10.51 mmol) 4-methylaminobenzoic acid methyl ester and 1.95 mL (14.0 mmol) triethylamine in 50 mL dichloromethane at 0 °C. The mixture was stirred for 16 h at room temperature and evaporated to give a white solid. The white solid was dissolved in ethyl acetate and washed using water, sodium bicarbonate, and finally with brine solution. The organic layer was dried over anhydrous sodium sulfate and evaporated to give a white solid product. Yield = 1.754 g (76.85%). <sup>1</sup>H NMR ( $\text{DMSO}-d_6$ ,  $\delta$  ppm): 3.27 (s, 9H, OMe-H), 3.89 (s, 9H, NMe-H), 6.79 (d, 6H, ArH), 7.04 (s, 3H, ArH), 7.85 (d, 6H, ArH).

**HYDROLYSIS OF *N,N',N''*-METHYL-4,4',4''-[1,3,5-BENZENETRIYLTRIS(CARBONYLIMINO)]TRISBENZOIC ACID METHYL ESTER.** 0.504 g (0.774 mmol) of *N,N',N''*-methyl-4,4',4''-[1,3,5-benzenetriyltris(carboxylimino)]trisbenzoic acid methyl ester was dissolved in ethanol (30 mL), and 10 mL 1 N NaOH aqueous solution was added to the solution. The mixture was stirred at ambient temperature for 1 h and evaporated to give a white solid. The solid was then dissolved in water and 1 M HCl solution was added dropwise to precipitate the white solid product. The product was filtered, washed using water and dried over phosphorus pentoxide. Yield = 0.293 g (62.1%). <sup>1</sup>H NMR ( $\text{DMSO}-d_6$ ,  $\delta$  ppm): 2.72 (s, 9H, Me-H), 3.32 (s, 9H, NMe-H), 6.43 (s, 3H, ArH), 6.52 (d, 6H, ArH), 7.67 (d, 6H, ArH), 11.97 (s, 3H, COOH). <sup>13</sup>C NMR ( $\text{DMSO}-d_6$ ,  $\delta$  ppm): 167.45, 153.34, 131.02, 116.62, 110.37 (br), 29.10. EA calc. for  $\text{H}_3\text{L}^2$  ( $\text{C}_{33}\text{H}_{27}\text{N}_3\text{O}_9$ , MW = 609.59 g mol<sup>-1</sup>): C, 65.02; H, 4.46; N, 6.89. Found: C, 65.17; H, 4.77; N, 6.88%.

**PREPARATION OF  $[\text{Cu}_3(\text{L}^1)_2(\text{H}_2\text{O})_3] \cdot 14\text{DMF} \cdot 16\text{H}_2\text{O}$ , 1.** 0.049 g (0.080 mmol) of  $\text{H}_3\text{L}^1$  was dissolved in 4 mL *N,N'*-dimethylformamide (DMF) and the solution was acidified with 0.7 mL 1 M  $\text{HNO}_3$  in a 10 mL vial. 0.034 g (0.16 mmol) of  $\text{Cu}(\text{NO}_3)_2 \cdot 6\text{H}_2\text{O}$  was added to the above solution. The vial was heated at 70 °C for 2 d. After cooling to room temperature, the cyan block-shaped crystals formed were filtered and soaked in fresh DMF. Yield = 0.106 g, 91.0%. EA calc. for  $[\text{Cu}_3(\text{L}^1)_2(\text{H}_2\text{O})_3] \cdot 14\text{DMF} \cdot 16\text{H}_2\text{O}$  ( $\text{Cu}_3\text{C}_{102}\text{H}_{178}\text{N}_{20}\text{O}_{51}$ , FW = 2687.98), 1: C, 45.52; H, 6.67; N, 10.41. Found: C, 45.31; H, 6.16; N, 10.80%. IR (KBr,  $\text{cm}^{-1}$ ): 3432, 3299, 2937, 1660, 1604, 1526, 1392, 1318, 1255, 1261, 1178, 1104, 862, 783, 731 and 662.

**PREPARATION OF  $[\text{Ni}_{14}(\mu^3\text{-OH})_8(\text{L}^2)_6(\text{FORMATE})_2(\text{DMF})_{10}(\text{H}_2\text{O})_2] \cdot 28\text{DMF} \cdot 14\text{H}_2\text{O}$ , 2.** 0.0061 g (0.010 mmol) of  $\text{H}_3\text{L}^2$  was dissolved in 1 mL DMF and 0.0060 g (0.021 mmol) of  $\text{Ni}(\text{NO}_3)_2 \cdot 6\text{H}_2\text{O}$  was added to the above solution. The green solution was placed in a glass tube, which was then sealed and heated to 120 °C in an oven. After 10 days, pale-green block-shaped crystals were formed. Yield = 0.0043 g, 33%. EA calc. for  $[\text{Ni}_{14}(\mu^3\text{-OH})_8(\text{L}^2)_6(\text{formate})_2(\text{DMF})_{10}(\text{H}_2\text{O})_2] \cdot 28\text{DMF} \cdot 14\text{H}_2\text{O}$  ( $\text{Ni}_{14}\text{C}_{314}\text{H}_{452}\text{N}_{56}\text{O}_{120}$ , FW = 7752.96), 2: C, 48.64; H, 5.88; N, 10.12. Found: C, 48.92; H, 6.31; N, 9.73%. IR (KBr,  $\text{cm}^{-1}$ ): 3441, 1653, 1602, 1559, 1393, 1178, 1109, 1018, 868, 792, 711 and 668.

### Crystallographic data collection and refinement of the structure

A crystal of **1** was coated with Paratone-N oil and the diffraction data were measured at 173 K using Mo K $\alpha$  radiation in an X-ray diffraction camera system using an imaging plate equipped with a graphite crystal incident beam monochromator. The Rapid Auto software package<sup>12</sup> was used for data collection and processing. A crystal of **2** was coated with Paratone-N oil and the diffraction data were collected at 96 K with synchrotron radiation ( $\lambda = 0.80000 \text{ \AA}$ ) on an ADSC Quantum-210 detector at 2-D SMC with a silicon (111) double crystal monochromator at the Pohang Accelerator Laboratory, Korea. The ADSC Q210 ADX program<sup>13</sup> was used for data collection (detector distance was 65 mm, omega scan;  $\Delta\omega = 2^\circ$ , exposure time was 20 s/frame) and HKL3000sm (Ver. 703r)<sup>14</sup> was used for cell refinement, reduction and absorption correction. Both structures were solved using direct methods employing the XS program of the SHELXTL PLUS software package<sup>15</sup> and refined using full-matrix least-squares calculations employing the XL program of the SHELXTL PLUS software package.

$[\text{Cu}_3(\text{L}^1)_2(\text{H}_2\text{O})_3]$ , **1**. A copper ion with a ligated water molecule on a crystallographic twofold axis and a ligand on a crystallographic threefold axis formed an asymmetric unit. All non-hydrogen atoms were refined anisotropically. The hydrogen atoms were assigned isotropic displacement coefficients  $U(\text{H}) = 1.2U(\text{C}$  and  $\text{N})$ , and their coordinates were allowed to ride on their respective atoms. The least-squares refinement of the structural model was performed under geometry restraints and displacement parameter restraints such as DFIX, DANG, AFIX, FLAT and ISOR. The final refinement was performed with the modification of the structure factors for the electron densities of the disordered solvent regions ( $25\,342 \text{ \AA}^3$ , 74.8% of the unit cell volume; 1902 solvent electrons [ $\sim 48$  DMF molecules] per unit cell) using the SQUEEZE option of PLATON.<sup>16</sup> The hydrogen atoms attached to the water molecules were not included in the least-squares refinement. Refinement converged at a final  $R_1 = 0.1515$  and  $wR_2 = 0.4379$  for 1605 reflections with  $I > 2\sigma(I)$ ;  $R_1 = 0.2465$  and  $wR_2 = 0.4844$  for all 4057 reflections. The largest differences peak and hole were 0.619 and  $-0.335 \text{ e \AA}^{-3}$ , respectively. Attempts to collect the better data sets were not successful because of the large unit cell dimensions and the extremely large solvent cavity.

$\text{Ni}_{14}(\mu^3\text{-OH})_8(\text{L}^2)_6(\text{FORMATE})_2(\text{DMF})_{10}(\text{H}_2\text{O})_2 \cdot 16(\text{DMF})$ , **2**. Seven nickel atoms, three ligands, one formate, four  $\mu^3$ -hydroxo oxygen atoms, five ligated DMF molecules, one ligated water molecule and eight additional DMF molecules as lattice solvent were observed as an asymmetric unit. All non-hydrogen atoms were refined anisotropically; the hydrogen atoms were assigned isotropic displacement coefficients  $U(\text{H}) = 1.2U(\text{C})$ ,  $1.5U(\text{C}_{\text{methyl}})$  and their coordinates were allowed to ride on their respective atoms. The least-squares refinement of the structural model was performed under geometry restraints such as DANG, DFIX and FLAT and displacement parameter restraint, ISOR, for some atoms of the statistically disordered ligand and the lattice DMF molecules. The hydrogen atoms attached on the hydroxo groups and the water molecule were not included in the structural model. The final refinement was

performed with the modification of the structure factors for the electron densities of the remaining disordered solvent regions ( $2142 \text{ \AA}^3$ , 6.7% of the unit cell volume; 480 solvent electrons [ $\sim 12$  DMF molecules] per unit cell) using the SQUEEZE option of PLATON. Refinement converged at a final  $R_1 = 0.0643$  and  $wR_2 = 0.1933$  for 19 568 reflections with  $I > 2\sigma(I)$ ;  $R_1 = 0.0803$  and  $wR_2 = 0.2031$  for all 26 217 reflections. The largest differences peak and hole were 0.668 and  $-0.425 \text{ e \AA}^{-3}$ , respectively.

A summary of the crystal data for **1** and **2** is given in Tables S1 and S2, ESI.†

## Results and discussion

A solvothermal reaction of  $\text{H}_3\text{L}^1$  with  $\text{Cu}(\text{NO}_3)_2 \cdot 6\text{H}_2\text{O}$  in DMF led to cyan block-shaped crystals of **1**. The single crystal structure analysis revealed that **1** was the twofold interpenetrated 3-D MOF,  $[\text{Cu}_3(\text{L}^1)_2(\text{H}_2\text{O})_3]$ , with a (3,4)-connected **pto** net topology, where the  $\text{H}_3\text{L}^1$  of the *trans*-amide conformation in an extended geometry served as a 3-connected node and the  $\text{Cu}(\text{II})$  paddle-wheel secondary building unit,  $\text{Cu}_2(\text{COO})_4$ , served as a planar 4-connected node (Fig. 1). As the 3-connected ligand conformations in the other MOFs of the **pto** net topology, the benzoate moieties of 3-connected  $\text{L}^1$  of **1** are twisted from the ligand plane with an angle of  $36.5(3)^\circ$ . The large pore dimension in the single network generated by

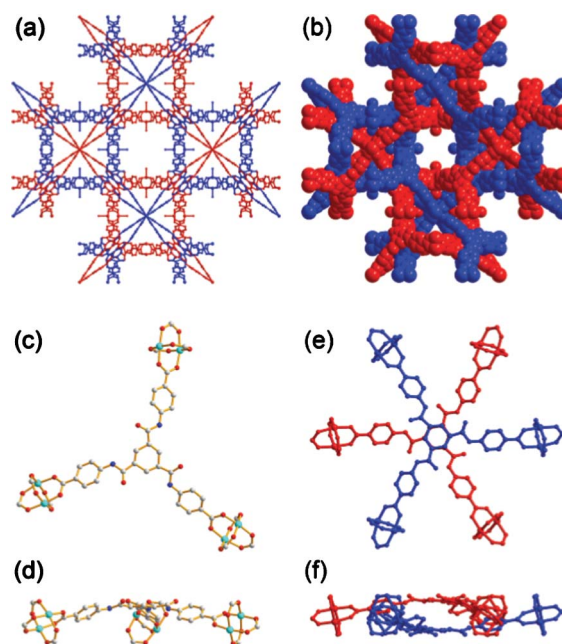


**Fig. 1** (a) Ball-and-stick and (b) space-filling diagrams of the twofold interpenetrated networks of **1**, using blue and red for the two interpenetrated networks, of a (3,4)-connected **pto** net topology; (c)  $\text{L}^1$  ligand unit as a 3-connected node and  $\text{Cu}_2(\text{COO})_4$  SBU as a planar 4-connected node in top view; (d) side view of the 3- and 4-connected nodes, where the carboxylates of the ligand are twisted from the central phenyl plane; (e) top and (f) side view of the  $\pi$ - $\pi$  stacking interactions of central phenyl rings between the interpenetrated networks.

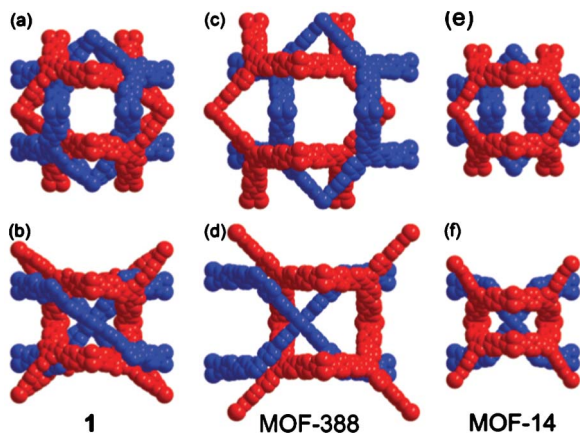


**Fig. 2** Interpenetration modes observed in the cage-like and the channel-like pores of **1** ((a) and (b)), of MOF-388 ((c) and (d)), and of MOF-14 ((e) and (f)), respectively.

flexible  $L^1$  ligand allowed the twofold interpenetration as in the MOFs with the same **pto** net topology with large pore dimension (Fig. 1a and 1b) such as MOF-14 made of 4,4',4''-(benzene-1,3,5-triyltribenzoic acid ( $H_3$ BTB) ligand<sup>6</sup> and MOF-388 made of 4,4',4''-triazine-2,4,6-triyl-tris-(benzene-4,1-diyl)-tribenzoic acid ( $H_3$ TAPB) ligand.<sup>7b</sup>

However, the twofold interpenetrated MOF, **1**, of space group  $Pn\bar{3}n$  is not isorecticular to the other two reported twofold interpenetrated MOFs with the same **pto** net topology, MOF-14 with space group  $Im\bar{3}$  and MOF-388 with space group  $P4_2/nmc$  (Fig. 2 and 3). The two interpenetrated networks in **1** are related to each other by crystallographic inversion symmetry, like the two interpenetrated networks in MOF-388.<sup>‡</sup> Even though both **1** and MOF-388 are related by the same crystallographic inversion symmetry, the interpenetration mode in **1** is not the same as that observed in MOF-388. The interpenetration mode of **1** is different from that of MOF-14, where the two interpenetrated networks are related to each other by the crystallographic  $(1/2, 1/2, 1/2)$  lattice translation.<sup>6</sup> The 3-connected nodes in the two idealized interpenetrating networks of **1** would collide; hence, the two central phenyl rings from the two interpenetrating networks are bowed to each other to avoid the collision observed in MOF-14, although there is no collision between the 3-connected nodes of the idealized interpenetrating networks of the same inversion-related but different interpenetration mode observed in MOF-388 (Fig. 4). The phenyl groups of the bowed ligands in **1** also interact *via* strong  $\pi$ - $\pi$  stacking, like those in MOF-14.

The interpenetrated networks in **1** with flexible  $L^1$  are more extensively interwoven than those in MOF-14 and MOF-388 with the more rigid ligands, BTB and TATB, respectively (Fig. 2 and 3). The twofold interpenetration in **1** has generated two different pore structures within the framework (Fig. 5). The pore diameter of the *interwoven* cage-like pore is  $\sim 21.4$  Å

<sup>‡</sup> In ref. 7b, the two interpenetrated networks were described as though they were not related by symmetry; they are related by crystallographic inversion symmetry.

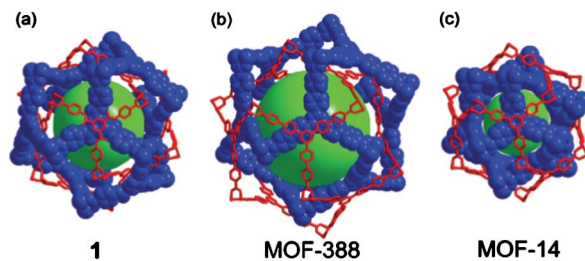


**Fig. 3** (a) The *interwoven* cage-like pore in **1**, (b) the partially *interwoven* cage-like pore in MOF-388, and (c) the *double shell* cage-like pore observed in MOF-14.

(Fig. 5a), which is substantially larger than the corresponding pore diameter of the *double shell* cage-like pore observed in MOF-14 ( $\sim 15.8$  Å) (Fig. 3). The *interwoven* cage-like pores in **1** are interconnected through six *interwoven* channel-like pores of  $\sim 6.0$  Å channel diameter (Fig. 5b-d). The total accessible solvent volume per unit cell of **1** (75%) calculated using the PLATON program is slightly larger than that of MOF-14 (67%). The bulk identity of as-synthesized **1** was confirmed by using powder X-ray diffraction (PXRD) (Fig. S1, ESI<sup>†</sup>), together with elemental analysis.

The removal of the solvent molecules from the pore *via* conventional vacuum drying before and after solvent exchange using volatile solvents resulted in the complete loss of crystallinity and the collapse of the porosity, leaving no significant  $N_2$  sorption properties. Even the effort to activate the sample using supercritical  $CO_2$  activation was not successful, which suggests that the ligand flexibility led to the loss of the porosity when the solvent molecules were removed from the framework, even though **1** was a twofold interpenetrated network.

A solvothermal reaction of  $H_3L^2$  with  $Ni(NO_3)_2 \cdot 6H_2O$  in DMF afforded pale-green block-shaped crystals of **2**. The single crystal X-ray structure analysis revealed that **2** is a finite

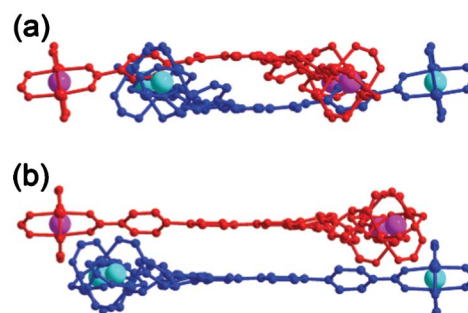


**Fig. 4** The side views of the 3-connected ligands with the 4-connected  $Cu_2(COO)_4$  SBUs in  $\pi$ - $\pi$  stacking interaction in the interpenetrating networks of (a) **1** and (b) MOF-388, where the centers of the 4-connected  $Cu_2(COO)_4$  SBUs from the two interpenetrating networks are represented using pink and cyan balls, respectively. Notice that  $L^1$  in **1** is bowed to avoid the collision at the ideal position of the two 3-connected ligands in the interpenetrating networks and TAPB in MOF-388 is flat because the ideal positions of the two 3-connected ligands are not colliding with each other.

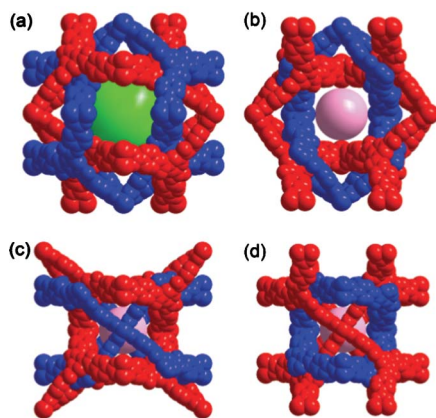


**Fig. 5** (a) The *interwoven* cage-like pore of **1** shown along the crystallographic *a*-axis; (b)–(d) the *interwoven* channel-like pore of **1** shown along the crystallographic *b*-axis, *a*-axis, and *c*-axis, respectively.

tetradecanuclear MOC with formula  $[\text{Ni}_{14}(\mu^3\text{-OH})_8(\text{L}^2)_6(\text{formate})_2(\text{DMF})_{10}(\text{H}_2\text{O})_2]$  (**2**) on a crystallographic inversion center consists of 14 Ni(II) metal ions that are bridged *via* eight  $\mu^3$ -hydroxo oxygen atoms (Fig. S2, ESI†).§ The  $\mu^3$ -hydroxo bridged tetradecanuclear cluster is further bridged by using 20 carboxylates, 18 from the six  $\text{L}^2$  units and two from

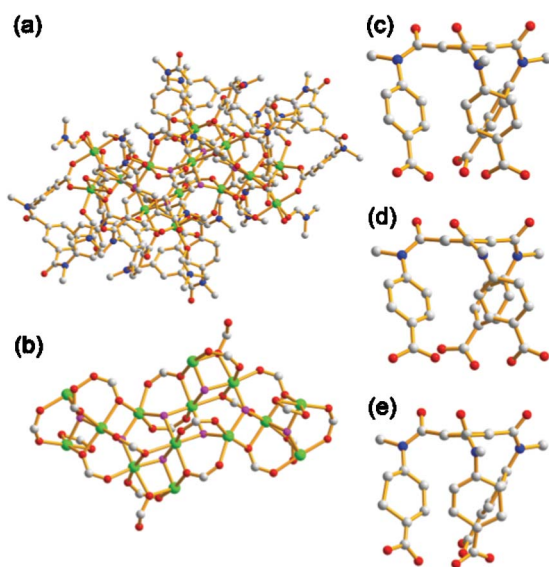


**Fig. 6** (a) Ball-and-stick diagram of  $[\text{Ni}_{14}(\mu^3\text{-OH})_8(\text{L}^2)_6(\text{formate})_2(\text{DMF})_{10}(\text{H}_2\text{O})_2]$ , **2**, where metal ions are surrounded by six  $\text{L}^2$  units, two formates, and solvent DMF and water molecules; (b) the core diagram of  $\text{Ni}_{14}$  MOC, showing only the metal ions together with  $\mu^3$ -hydroxo and carboxylato groups; (c)–(e) three  $\text{L}^2$  units of a tripodal geometry in chemically different environments with all benzamides in *cis*-conformation. Color codes: nickel, green; carbon, gray; nitrogen, blue;  $\mu^3$ -hydroxo oxygen, pink; other oxygen, red.

§ All the bridging oxygen atoms in the crystal structure of **2** were assigned as  $\mu^3$ -hydroxo groups based on their pyramidal geometry and considering the charge balance of the whole structure.

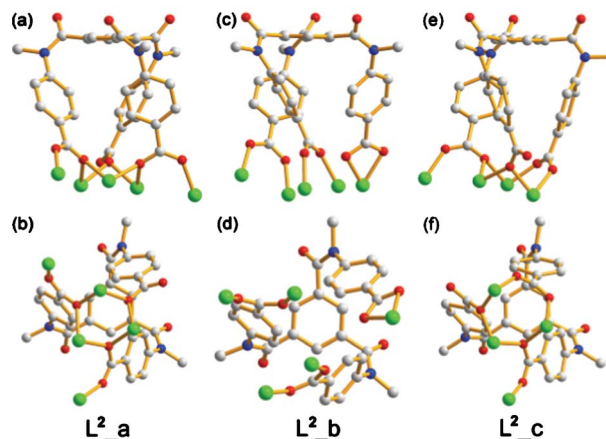


**Fig. 7** Ball-and-stick representation of the three different  $\text{L}^2$  units ( $\text{L}^2_{\text{a}}$ ,  $\text{L}^2_{\text{b}}$ , and  $\text{L}^2_{\text{c}}$ ) observed in **2** in various metal binding modes: (a) and (b) for  $\text{L}^2_{\text{a}}$ , (c) and (d) for  $\text{L}^2_{\text{b}}$ , and (e) and (f) for  $\text{L}^2_{\text{c}}$  as side view and top view, respectively.

the formates that are generated *in situ* during the reaction *via* the dissociation of DMF (Fig. 6b). The solvent DMF and water molecules are ligated on the remaining coordinate sites of the Ni(II) centers of the six-coordinate octahedral coordination geometry (Fig. 6a). The distance between the adjacent Ni(II) centers varies, in the range 2.961(1)–3.638(1) Å, depending upon the bridging modes of the hydroxo and carboxylato groups. All three crystallographically unique ligands of different chemical environments in **2** are in the expected folded tripodal geometry with all the tertiary benzamide linkages in *cis*-conformation (Fig. 6c–e). The folded geometry keeps all three carboxylates of the ligand in close proximity in space and the proximal carboxylates render the finite high-nuclearity MOC with the extensively bridged carboxylates in various bridging modes (Fig. 7). **2** is one of a handful of polynuclear Ni MOCs with a nuclearity equal to or larger than 14.<sup>17</sup> The bulk identity of as-synthesized **2** was also confirmed by using PXRD (Fig. S3, ESI†), together with elemental analysis.

## Conclusions

We have successfully demonstrated a strategy for the synthesis of a finite MOC and an extended MOF simply by controlling the conformation of the ligand.  $\text{H}_3\text{L}^2$  with all benzamide linkages in *cis*-conformation and with a folded geometry served as a folded tripodal ligand. The reaction of the folded ligand with Ni(II) led to a finite MOC, where all three carboxylates from the same ligand are in close proximity in space and are involved in extensive and various bridging modes. On the other hand,  $\text{H}_3\text{L}^1$  with all benzamide linkages in *trans*-conformation and with an extended geometry served as a 3-connected node. The combination of the ligand in the extended geometry with Cu(II) ion generates a planar 4-connected  $\text{Cu}_2(\text{COO})_4$  SBU to form a (3,4)-connected 3-D MOF. Although the flexibility of the amide linkages of the ligand could allow the carboxylates to be in the ligand plane to form a

3-D network with a **tbo** net topology, all the carboxylates are in twisted conformations from the ligand plane. The combination of the ligand in the twisted conformation with a planar 4-connected  $\text{Cu}_2(\text{COO})_4$  SBU forms an extensively interwoven 3-D framework with a **pto** net topology with a twofold interpenetration mode.

An appropriate choice of functionalities can direct the same class of building blocks to different conformations. The geometries of tricarboxylate ligands controlled *via* the conformation of the benzamide linkage could be utilized for the construction of a finite MOC or an extended 3-D MOF. This work will encourage the investigation of similar synthetic approaches for the preparation of MOCs and MOFs.

## Acknowledgements

This work was supported by NRF-2011-0027950, NRF-2012-003077 and WCU programs (R31-2011-000-20012-0) through the National Research Foundation of Korea. The authors acknowledge PAL for beam line use (2012-1st-2D-014).

## References

- (a) D. L. Caulder and K. N. Raymond, *Acc. Chem. Res.*, 1999, **32**, 975; (b) M. Fujita, M. Tominaga, A. Hori and B. Therrien, *Acc. Chem. Res.*, 2005, **38**, 371; (c) D. J. Tranchemontagne, Z. Ni, M. O'Keeffe and O. M. Yaghi, *Angew. Chem., Int. Ed.*, 2008, **47**, 5136; (d) R. Chakrabarty, P. S. Mukherjee and P. J. Stang, *Chem. Rev.*, 2011, **111**, 6810.
- (a) M. O'Keeffe, M. Eddaoudi, H. Li, T. Reineke and O. M. Yaghi, *J. Solid State Chem.*, 2000, **152**, 3; (b) N. W. Ockwig, O. Delgado-Friedrichs, M. O'Keeffe and O. M. Yaghi, *Acc. Chem. Res.*, 2005, **38**, 176; (c) O. Delgado-Friedrichs, M. O'Keeffe and O. M. Yaghi, *Acta Crystallogr., A: Found. Crystallogr.*, 2006, **62**, 350; (d) M. O'Keeffe, M. A. Peskov, S. J. Ramsden and O. M. Yaghi, *Acc. Chem. Res.*, 2008, **41**, 1782; (e) M. O'Keeffe and O. M. Yaghi, *Chem. Rev.*, 2012, **112**, 675; (f) V. A. Blatov, L. Carlucci, G. Ciani and D. M. Proserpio, *CrystEngComm*, 2004, **6**, 377.
- (a) D. Fiedler, D. H. Leung, R. G. Bergman and K. N. Raymond, *Acc. Chem. Res.*, 2005, **38**, 351; (b) T. C. Stamatatos, K. A. Abboud, W. Wernsdorfer and G. Christou, *Angew. Chem., Int. Ed.*, 2007, **46**, 884; (c) L. Bogani and W. Wernsdorfer, *Nat. Mater.*, 2008, **7**, 179.
- (a) M. P. Suh, H. J. Park, T. K. Prasad and D.-W. Lim, *Chem. Rev.*, 2012, **112**, 782; (b) K. Sumida, D. L. Rogow, J. A. Mason, T. M. McDonald, E. D. Bloch, Z. R. Herm, T.-H. Bae and J. R. Long, *Chem. Rev.*, 2012, **112**, 724; (c) J.-R. Li, J. Sculley and H.-C. Zhou, *Chem. Rev.*, 2012, **112**, 869; (d) M. Yoon, R. Srirambalaji and K. Kim, *Chem. Rev.*, 2012, **112**, 1196; (e) L. E. Kreno, K. Leong, O. K. Farha, M. Allendorf, R. P. Van Duyne and J. T. Hupp, *Chem. Rev.*, 2012, **112**, 1105; (f) Y. Cui, Y. Yue, G. Qian and B. Chen, *Chem. Rev.*, 2012, **112**, 1126; (g) C. Wang, T. Zhang and W. Lin, *Chem. Rev.*, 2012, **112**, 1084; (h) D. Zacher, O. Shekhah, C. Wöll and R. A. Fischer, *Chem. Soc. Rev.*, 2009, **38**, 1418; (i) M. Kurmoo, *Chem. Soc. Rev.*, 2009, **38**, 1353.
- (a) S. S.-Y. Chui, S. M.-F. Lo, J. P. H. Charmant, A. G. Orpen and I. D. Williams, *Science*, 1999, **283**, 1148; (b) L. J. Murray, M. Dinca, J. Yano, S. Chavan, S. Bordiga, C. M. Brown and J. R. Long, *J. Am. Chem. Soc.*, 2010, **132**, 7856; (c) D. Sun, S. Ma, Y. Ke, D. J. Collins and H.-C. Zhou, *J. Am. Chem. Soc.*, 2006, **128**, 3896; (d) S. Ma, D. Sun, M. Ambrogio, J. A. Fillinger, S. Parkin and H.-C. Zhou, *J. Am. Chem. Soc.*, 2007, **129**, 1858; (e) X.-S. Wang, S. Ma, D. Yuan, J. W. Yoon, Y. K. Hwang, J.-S. Chang, X. Wang, M. R. Jørgensen, Y.-S. Chen and H.-C. Zhou, *Inorg. Chem.*, 2009, **48**, 7519; (f) X.-S. Wang, S. Ma, D. Sun, S. Parkin and H.-C. Zhou, *J. Am. Chem. Soc.*, 2006, **128**, 16474.
- B. Chen, M. Eddaoudi, S. T. Hyde, M. O'Keeffe and O. M. Yaghi, *Science*, 2001, **291**, 1021.
- (a) S. Amirjalayer, M. Tafipolsky and R. Schmid, *J. Phys. Chem. C*, 2011, **115**, 15133; (b) H. Furukawa, Y. B. Go, N. Ko, Y. K. Park, F. J. Uribe-Romo, J. Kim, M. O'Keeffe and O. M. Yaghi, *Inorg. Chem.*, 2011, **50**, 9147.
- S. P. Argent, A. Greenaway, M. C. Gimenez-Lopez, W. Lewis, H. Nowell, A. N. Khlobystov, A. J. Blake, N. R. Champness and M. Schröder, *J. Am. Chem. Soc.*, 2012, **134**, 55.
- (a) K. Yamaguchi and G. Matsumura, *J. Am. Chem. Soc.*, 1991, **113**, 5474; (b) A. Itai, Y. Toriumi, S. Saito, H. Kagechika and K. Shudo, *J. Am. Chem. Soc.*, 1992, **114**, 10649; (c) F. D. Lewis, T. M. Long, C. L. Stern and W. Liu, *J. Phys. Chem. A*, 2003, **107**, 3254; (d) N. L. S. Yue, M. C. Jennings and R. J. Puddephatt, *Inorg. Chem.*, 2005, **44**, 1125.
- X. Song, Y. Zou, X. Liu, M. Oh and M. S. Lah, *New J. Chem.*, 2010, **34**, 2396.
- Materials Studio program, version 4.3*, Accelrys, San Diego, CA, 2008.
- Rapid Auto software, R-Axis series*, Cat. No. 9220B101, Rigaku Corporation.
- A. J. Arvai and C. Nielsen, *ADSC Quantum-210 ADX Program*, Area Detector System Corporation, Poway, CA, USA, 1983.
- Z. Otwinowski and W. Minor, in *Methods in Enzymology*, ed. C. W. Carter Jr. and R. M. Sweet, Academic Press, New York, 1997, **vol. 276**, p. 307.
- G. M. Sheldrick, SHELX program, *Acta Crystallogr., Sect. A*, 2008, **64**, 112.
- A. L. Spek, PLATON program, *Acta Crystallogr., Sect. A: Found. Crystallogr.*, 1990, **46**, 194.
- (a) A. L. Dearden, S. Parsons and R. E. P. Winpenney, *Angew. Chem., Int. Ed.*, 2001, **40**, 155; (b) M. Murrie, H. Stoeckli-Evans and H.-U. Güdel, *Angew. Chem., Int. Ed.*, 2001, **40**, 2011; (c) D. Foguet-Albiol, K. A. Abboud and G. Christou, *Chem. Commun.*, 2005, 4282; (d) T. C. Stamatatos, A. Escuer, K. A. Abboud, C. P. Raptopoulou, S. P. Perlepes and G. Christou, *Inorg. Chem.*, 2008, **47**, 11825; (e) J. Esteban, L. Alcázar, M. Torres-Molina, M. Monfort, M. Font-Bardia and A. Escuer, *Inorg. Chem.*, 2012, **51**, 5503.